DISCRETE AND CONTINUOUS
DYNAMICAL SYSTEMS SERIES S
Volume **4**, Number **5**, October **2011**

doi:10.3934/dcdss.2011.4.1213

pp. **1213–1225**

DISSIPATIVE SOLITONS IN BINARY FLUID CONVECTION

Isabel Mercader, Oriol Batiste and Arantxa Alonso

Departament de Física Aplicada, Universitat Politècnica de Catalunya
Campus Nord, 08034 Barcelona, Spain

Edgar Knobloch

Department of Physics, University of California
California, Berkeley, CA 94720, USA

Abstract. A horizontal layer containing a miscible mixture of two fluids can produce dissipative solitons when heated from below. The physics of the system is described, and dissipative solitons are computed using numerical continuation for three distinct sets of experimentally realizable parameter values. The stability of the solutions is investigated using direct numerical integration in time and related to the stability properties of the competing periodic state.

1. **Introduction.** Many fluid systems exhibit spatially localized structures in both two [2, 4, 5, 7, 9, 14, 16] and three [10, 23] dimensions. Of these the localized structures or *convectons* arising in binary fluid convection are perhaps the best studied. These states are similar to localized structures studied in other areas of physics [1] despite the fact that fluid systems must always be confined between boundaries. On the other hand in fluid systems the length scale is typically set by the layer depth or the distance between any confining boundaries instead of being an intrinsic length scale selected by a Turing or modulational instability. As a result when we speak of localized states in binary fluid convection we mean states that are localized in the horizontal direction only. In this sense the problem resembles laser systems in short cavities in which the standing wave structure in the longitudinal direction remains of paramount importance [15].

In fluids dissipation, whether through viscosity or thermal diffusion, is generally of great importance. For example, it is responsible for the presence of a finite threshold value of the Rayleigh number, a dimensionless measure of thermal forcing, for convection to occur. As a result the solitons of interest in the present article are strongly dissipative and hence require strong forcing for their maintenance. States of this type cannot therefore be understood in terms of (an infinite-dimensional) Hamiltonian system with small forcing and dissipation.

In this paper we study localized states in binary fluid convection in a horizontal layer of depth h heated from below. Binary liquids, such as water-ethanol and water-salt mixtures or mixtures of He^3-He^4 at cryogenic temperatures, are characterized by a cross-diffusion effect called the Soret effect that describes the diffusive separation

2000 *Mathematics Subject Classification.* Primary: 74J35, 76E0634; Secondary: 34K18, 34C37.

Key words and phrases. Dissipative solitons, binary fluid convection, bifurcation theory.

This work was supported in part by the National Science Foundation under grant DMS-0605238, DGICYT under grant FIS2006-08954 and by AGAUR under grant 2005SGR-0024.

of the lighter and heavier molecular weight components of the mixture in an imposed temperature gradient. When the Soret coefficient is positive the heavier component migrates, on a diffusive time scale, towards the colder boundary and vice versa. On the other hand in the anomalous case in which the Soret coefficient is negative the heavier component migrates towards the hotter boundary. As a result if a mixture with a negative Soret coefficient is heated from below the destabilizing temperature gradient sets up, in addition, a stabilizing concentration distribution. The competition between these two effects leads to complex behavior, including time-dependence at onset of convection.

We nondimensionalize the governing equations using the depth h as the unit of length and the thermal diffusion time h^2/κ in the vertical as the unit of time. The system is then described by the dimensionless equations [5]

$$\mathbf{u}_t + (\mathbf{u}\cdot\nabla)\mathbf{u} = -\nabla P + \sigma R[(1+S)\theta - S\eta]\hat{\mathbf{z}} + \sigma\nabla^2\mathbf{u}, \tag{1}$$

$$\theta_t + (\mathbf{u}\cdot\nabla)\theta = w + \nabla^2\theta, \tag{2}$$

$$\eta_t + (\mathbf{u}\cdot\nabla)\eta = \tau\nabla^2\eta + \nabla^2\theta, \tag{3}$$

together with the incompressibility condition $\nabla\cdot\mathbf{u} = 0$. Here $\mathbf{u} \equiv (u, w)$ is the dimensionless velocity field in (x, z) coordinates and P is the pressure. The quantity θ denotes the departure of the temperature from its conduction profile, in units of the imposed temperature difference ΔT, while η is defined such that its gradient represents the dimensionless diffusive flux of the heavier component, $\eta \equiv \theta - \Sigma$, where $C \equiv 1 - z + \Sigma$ is the concentration of the heavier component in units of the concentration difference that develops across the layer via the Soret effect in response to the imposed ΔT. The boundary conditions are thus $\mathbf{u} = \theta = \eta_z = 0$ on $z = 0, 1$, corresponding to no-slip, fixed temperature, zero-mass-flux boundaries at top and bottom. Throughout this paper we employ periodic boundary conditions in the horizontal direction, with the (dimensionless) spatial period Γ sufficiently large to permit the formation of dissipative solitons.

In addition to Γ the system (1)-(3) is specified by four dimensionless parameters,

$$R \equiv \frac{\alpha g \Delta T h^3}{\kappa\nu}, \quad S \equiv \frac{\beta}{\alpha} C_0(1-C_0)S_T, \quad \sigma \equiv \frac{\nu}{\kappa}, \quad \tau \equiv \frac{D}{\kappa}, \tag{4}$$

referred to, respectively, as the Rayleigh number, separation ratio, the Prandtl number and the Lewis number. Here $\alpha \equiv -\rho_0^{-1}(\partial\rho/\partial T)_0 > 0$ is the coefficient of thermal expansion, $\beta \equiv \rho_0^{-1}(\partial\rho/\partial C)_0 > 0$ is the corresponding coefficient describing the concentration dependence of the fluid density ρ, g is the acceleration due to gravity, ν is the kinematic viscosity and D is the molecular diffusivity of the heavier component. Thus σ and τ specify the properties of the fluid (typically for liquids $\sigma = O(1)$ while $\tau = O(10^{-2})$), while the parameter R specifies the strength of the applied temperature difference imposed across the system, and plays the role of an easily controllable bifurcation parameter. The parameter S is proportional to the Soret coefficient S_T and characterizes the mixture since it measures the concentration contribution to the buoyancy force due to cross-diffusion. When S or equivalently S_T is sufficiently negative, (i) the primary steady state bifurcation becomes subcritical since any convection that mixes the two components will decrease the stabilizing effect of the concentration stratification produced in response to the destabilizing thermal stratification, and hence make convection easier, and (ii) the primary instability of the conduction state $\mathbf{u} = \theta = \eta = 0$ becomes a Hopf bifurcation. This bifurcation is indicated in Fig. 1(a) by a solid dot, and in domains of

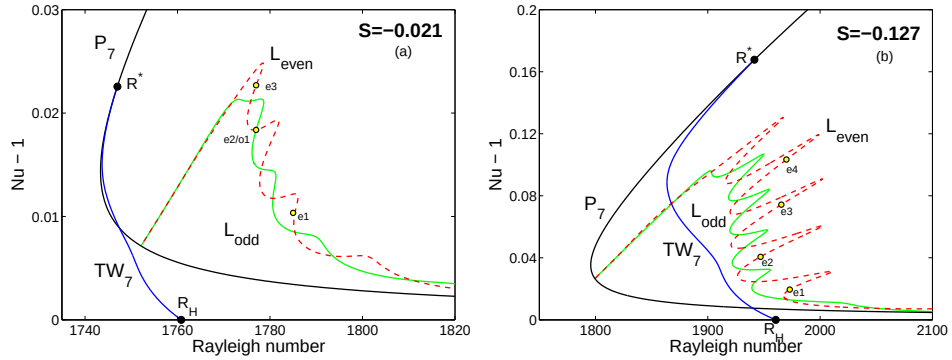

FIGURE 1. Bifurcation diagrams in a periodic domain with period $\Gamma = 14$ for (a) $\sigma = 6.22$, $\tau = 0.009$, $S = -0.021$ (Case A), (b) $\sigma = 6.86$, $\tau = 0.0083$, $S = -0.127$ (Case B), showing the normalized convective Nusselt number $\mathrm{Nu} - 1 \equiv \Gamma^{-1} \int_{-\Gamma/2}^{\Gamma/2} \partial_z \theta(x, z = 1)\, dx$ as a function of the Rayleigh number R for stationary periodic convection (P_7) and stationary spatially localized states of even ($\mathrm{L}_{\mathrm{even}}$, dashed line) and odd ($\mathrm{L}_{\mathrm{odd}}$, solid line) parity. The branch of traveling waves (TW_7) is also shown. The P_7 branch is stable for $R > R^*$.

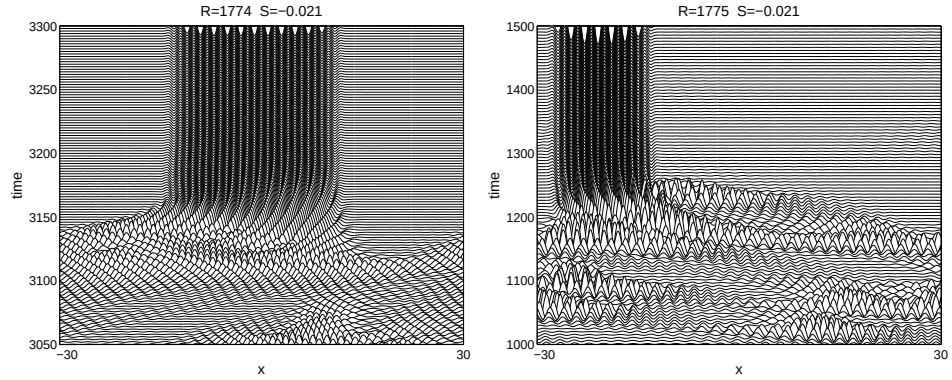

FIGURE 2. Space-time plots showing the midplane temperature $\theta(x, z = 1/2, t)$ for Case A as a function of time for (a) $R = 1774$, (b) $R = 1775$, starting from random small amplitude initial conditions in a $\Gamma = 60$ domain.

sufficiently large horizontal extent leads to a spatio-temporally chaotic state known as dispersive chaos [11, 22]. The time-independent convectons discussed here emerge from this state via relaxation oscillations as described in [5]. Figure 2 highlights the focusing instability of the dispersive chaos state that leads to the formation of stable convectons in large domains. Since these states emerge from a chaotic state the width of the convectons that result is not unique, and simulations starting from different small amplitude perturbations of the conduction state may result in convectons of different lengths even for identical parameter values.

With identical boundary conditions at top and bottom, as in the present system, the convectons are of two symmetry types, even and odd. Both types are present together in an interval of Rayleigh numbers called the pinning or snaking region [28] and may be stable [5]. The properties and organization of these states resemble those familiar from parallel studies of a much simpler problem, the Swift-Hohenberg equation on the real line:

$$u_t = ru - (\partial_x^2 + 1)^2 u + b_3 u^3 - u^5, \tag{5}$$

hereafter SH35 [12]. Figure 3 shows a typical bifurcation diagram computed for $b_3 = 2$ on a large domain of length Γ with periodic boundary conditions. The branch P of spatially periodic states with wavelength 2π bifurcates subcritically from $u = 0$ at $r = 0$ and is therefore initially unstable. With increasing amplitude it turns around and acquires stability in a saddle-node bifurcation. At point M, the Maxwell point, the energy of the state P vanishes and is therefore equal to the energy of the trivial state $u = 0$. At this point, $r = r_M$, fronts can be constructed connecting the $u = 0$ state to P and back again, and consequently steady spatially localized structures of arbitrary length all coexist. However, because the state P is structured, the fronts cannot move freely when r is perturbed from r_M: the fronts are pinned to the heterogeneity of the state P between them [28], and consequently will only move once $|r - r_M|$ becomes sufficiently large. This physical argument relies on the existence of a free energy for SH35 but explains why multiple distinct spatially localized equilibria should be present in a "pinning region" surrounding the Maxwell point.

There are in fact four distinct branches of dissipative solitons, labeled L_ϕ, that bifurcate from $u = 0$ simultaneously with the P branch (Fig. 3). Two of these are of even parity, with L_0 having maxima at the symmetry point $x = 0$, and L_π having minima at $x = 0$. In contrast, the odd parity solitons are characterized by $\phi = \pi/2$ (negative slope at $x = 0$) and $\phi = 3\pi/2$ (positive slope at $x = 0$). The $\phi = 0, \pi$ solitons are related by the symmetry $u \to -u$ of SH35 and likewise for the $\phi = \pi/2, 3\pi/2$ solitons. As a result the branches L_0, L_π in Fig. 3 coincide as do the branches $\mathrm{L}_{\pi/2}$ and $\mathrm{L}_{3\pi/2}$. At small amplitude these localized structures are only weakly localized (Fig. 3, panels (i)-(iv)), but become strongly localized by the time they enter the pinning region (Fig. 3, panels (v)-(viii)). Once in the pinning region all four soliton branches begin to snake, adding extra oscillations on either side of each soliton profile while preserving the overall symmetry of the profile (Fig. 3, panels (ix)-(xii)). Stability computations indicate that solitons on branches with a positive slope are stable (solid lines) while those on branches with a negative slope are unstable (dotted lines) [12]. Asymmetric solitons, located on the rungs connecting the even and odd snaking branches, are never stable.

Figures 1(a,b) show that much of the phenomenology associated with the pinning region as described by SH35 also applies to convection in binary mixtures. This is so despite the fact that the fluid problem is not variational in time, and no energy playing the role of a Lyapunov function can be defined. This is because the snaking behavior shown in Figs. 1(a,b) and in Fig. 3 is in fact a consequence of the formation of a heteroclinic *cycle* between a trivial (conduction) state and a periodic state (convection), i.e., a solution profile that connects the trivial state to the periodic state, with a second connection from the periodic state back to the trivial state as x increases. In generic systems the formation of this type of orbit is a higher codimension phenomenon but in systems that are *reversible* in space

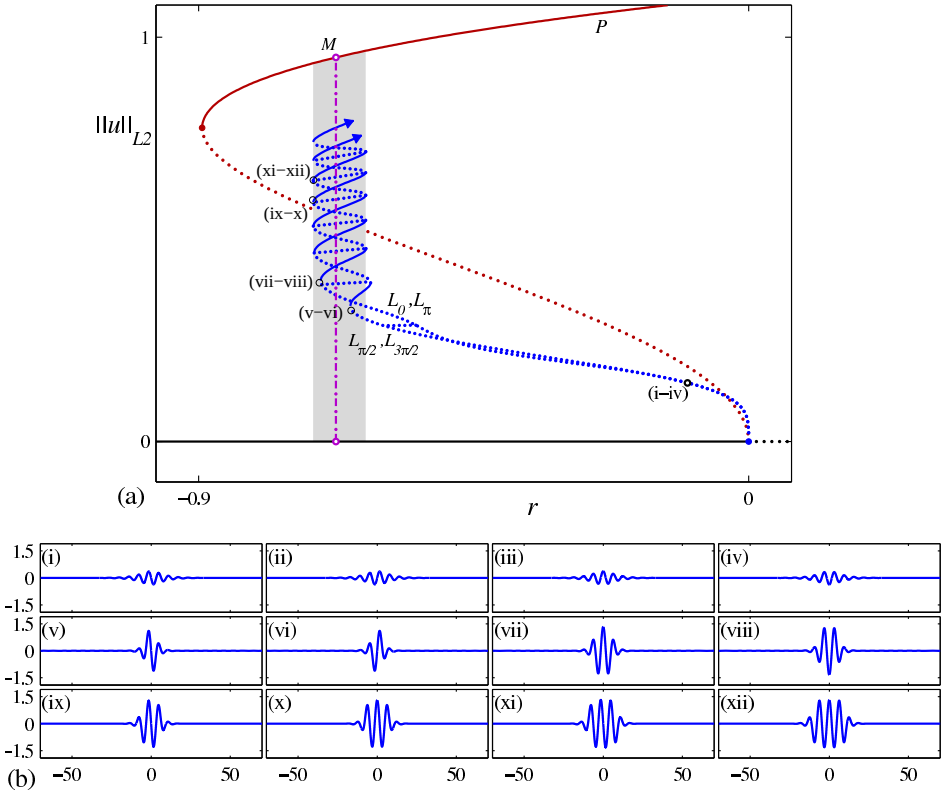

FIGURE 3. Bifurcation diagram for the Swift-Hohenberg equation SH35 showing the norm $||u||_{L^2} \equiv \Gamma^{-1} \int_{-\Gamma/2}^{\Gamma/2} u^2 \, dx$ of periodic states (P) with wavelength 2π, and two pairs of branches of even (L_0, L_π) and odd ($L_{\pi/2}$, $L_{3\pi/2}$) parity, all of which bifurcate together from $u = 0$ at $r = 0$ as $\Gamma \to \infty$. The pinning region containing stable (solid line) and unstable (dotted line) localized structures is shaded. (b) Sample profiles $u(x)$. First row, left to right: profiles near onset on $L_{\pi/2}$, $L_{3\pi/2}$, L_0, L_π. Second row: profiles at the first saddle-node on $L_{\pi/2}$, $L_{3\pi/2}$, L_0, L_π. Third row: profiles at the third saddle-nodes on $L_{\pi/2}$, L_0 and fifth saddle-nodes on $L_{\pi/2}$, L_0. The unstable rung states correspond to states that are neither even nor odd (profiles not shown). After [12].

the return connection follows from the equivariance of the equations with respect to $x \to -x$, and the heteroclinic cycle may become generic or *structurally stable*. Numerical computations suggest that this is the case for binary fluid convection: the pinning or snaking interval is filled with heteroclinic cycles connecting the trivial and periodic states. The boundaries of this region correspond to tangencies between the unstable (stable) manifold of the conduction state and the center-stable (center-unstable) manifold of the periodic state [6, 13, 29]; an energy function is not required at any stage of this argument. Moreover, the midplane reflection symmetry of Eqs. (1)-(3) with identical boundary conditions at top and bottom plays the same role as the symmetry $u \to -u$ of SH35. Consequently four branches of spatially

localized convectons bifurcate from the conduction state together with the branch P of periodic states, provided only that the problem is posed on the whole real line. When these are followed numerically by decreasing the Rayleigh number their amplitude grows while their width shrinks. Once their amplitude and width is comparable to the amplitude and wavelength of steady spatially periodic convection on the upper branch (Fig. 1a) all four convecton branches enter the pinning region and begin to snake back and forth across it (Fig. 1a) as the convectons grow in length by nucleating additional convection rolls at both ends. With periodic boundary conditions in the horizontal this process continues until the length of the convecton becomes comparable to the available spatial domain when the convecton branches turn over towards the saddle-node of the periodic branch and leave the pinning region [2, 7, 8]. The latter bifurcation can be interpreted as a bifurcation of holes from a periodic state, and once again creates four branches, with phases $\phi' = 0, \pi/2, \pi, 3\pi/2$. These branches also snake once they enter the pinning region from above, and the hole deepens and gradually fills with the conduction state. On the real line these eight snaking branches remain distinct but on periodic domains with finite period they (generally) connect pairwise [8]. We mention that we expect rung-like secondary branches to be present in Figs. 1(a,b) as well. However, in contrast to SH35 (Fig. 3), in the convection problem these states are expected to correspond to drifting solitons and these are not computed in this article – states of this type are only stationary in SH35 because of its variational structure.

In this article we study the above problem in two spatial dimensions, with a single extended horizontal dimension. We present results for three sets of parameters that have been used in experiments on water-ethanol mixtures. The computations use a periodic domain with $\Gamma = 14$, allowing exactly seven wavelengths of the periodic convection pattern in the computational domain. While not large, this aspect ratio suffices to identify and study single-pulse spatially localized structures that are of interest here. Nonperiodic domains with realistic lateral boundary conditions are discussed in detail in [25, 26].

2. **Results.** Steady solutions of Eqs. (1)–(3) with the boundary conditions specified above satisfy either $(u(x,z), w(x,z), \theta(x,z), \eta(x,z)) = (-u(-x,z), w(-x,z), \theta(-x,z), \eta(-x,z))$, or $(u(x,z), w(x,z), \theta(x,z), \eta(x,z)) = -(u(-x,1-z), w(-x,1-z), \theta(-x,1-z), \eta(-x,1-z))$. In the following we refer to the former as even and the latter as odd, in both cases with respect to the line $x = 0$. Since we are using periodic boundary conditions both the periodic states and the localized states can be translated so as to possess well-defined parity with respect to the center of the domain $x = 0$. Such states can therefore be computed by imposing appropriate symmetry on the solution. These symmetry properties are not, however, satisfied by time-dependent states such as the traveling wave states that bifurcate from the conducting state at $R = R_H$ (see Fig. 1). Instead these states have a mirror-glide symmetry [18, 3, 22]: $(u(x+\lambda/2,z), w(x+\lambda/2,z), \theta(x+\lambda/2,z), \eta(x+\lambda/2,z)) = (u(x,1-z), -w(x,1-z), -\theta(x,1-z), -\eta(x,1-z))$, at each instant of time, where λ is the wavelength of the traveling wave. Moreover, translations of the solution are equivalent to evolution in time. Solutions with this property are called rotating waves, since they correspond to steady states in an appropriately moving frame. The speed of this frame (the phase speed of the wave) solves a nonlinear eigenvalue problem. Care must be taken to include an overall mean flow in the horizontal direction that is associated with the wave. In dissipative systems of this type this mean

flow cannot be transformed away by a Galilean transformation and consequently all traveling states generically exhibit left-right asymmetric profiles – in contrast to classical problems such as the Korteweg-de Vries equation that is derived from a Galilean-invariant problem.

In the following we focus on three different parameter sets we refer to as Case A, B and C, respectively, and (i) compute the complete bifurcation diagrams for steady spatially localized states, and (ii) use direct numerical integration to determine the stability properties of these states in a $\Gamma = 14$ periodic domain. All three cases correspond to parameter values used in water-ethanol experiments although these typically employ larger aspect ratios than used in our numerical computations. Numerical continuation for these parameter sets has been carried out before but focused on periodic states with period $\Gamma = 2$ only, i.e., on steady overturning convection (hereafter SOC [5, 22]) and on traveling wave convection (hereafter TW [22, 24]) with wavelength $\lambda = \Gamma$, and on their linear stability properties with respect to wavelength changing or Eckhaus modes [22]. Direct numerical integration in time was used to explore the evolution of this instability [22] and to locate stable localized structures [5]. Our continuation results broaden significantly the parameter space in which spatially localized states are known to be present [5]. A different set of parameter values was used in two recent studies of convectons in closed two-dimensional containers [25, 26].

2.1. **Case A: $\sigma = 6.22$, $\tau = 0.009$, $S = -0.021$.** Figure 1(a) shows the result of numerical branch following in a periodic domain of length $\Gamma = 14$ for the parameter values used in [21]. The branches of even and odd convectons (labeled $\mathrm{L_{even}}$, $\mathrm{L_{odd}}$) are shown in dashed and solid lines, respectively. Both branches terminate together on the branch P_7 of stationary periodic states with $n = 7$ pairs of rolls, just below the saddle-node on the latter. The figure also shows the branch of subcritical traveling waves TW_7 with seven wavelengths within the period Γ that bifurcate from the Hopf point at $R = R_H \approx 1760.81$ and terminate on P_7 at $R = R^* \approx 1746.96$. The bifurcation at $R = R^*$ corresponds to a (supercritical) parity-breaking bifurcation from a circle of equilibria (the state P_7) that produces (stable) TW that drift slowly in one or other direction; the phase speed of these waves approaches zero as $(R^* - R)^{1/2}$. For $R < R^*$ the (upper) P_7 branch is unstable to TW disturbances, while for $R > R^*$ it is stable with respect to both TW and amplitude perturbations, i.e., perturbations with the same symmetry as the state. Thus for these parameter values the pinning or snaking region is located in a range of Rayleigh numbers in which extended convectons resemble a part of a *stable* stationary periodic state. For these parameter values we expect to find stable convectons.

Figure 4(a) shows an even parity convecton at $R = 1785$ (top panel). This solution is located at $e1$ in Fig. 1(a), on a portion of $\mathrm{L_{even}}$ that in SH35 would correspond to stable solitons [12]. However, this is not the case here, as shown by the time trace of the vertical velocity component $w(-4.8, 0.78, t)$ (middle panel). This panel shows that this convecton is in fact unstable to infinitesimal perturbations and evolves into steady spatially periodic convection on the P_7 branch (bottom panel). Figure 4(b) shows for comparison an even parity convecton at $e2$ ($R = 1777$). This convecton is expected to be unstable with respect to amplitude perturbations [12] and is indeed unstable. The bottom panel shows that it evolves into a numerically stable odd parity convecton on $\mathrm{L_{odd}}$. In projection this final state almost coincides with the initial location $e2$ but lies on a portion of $\mathrm{L_{odd}}$ that is expected to be stable. We have also confirmed that a longer even parity convecton, at $e3$ (also

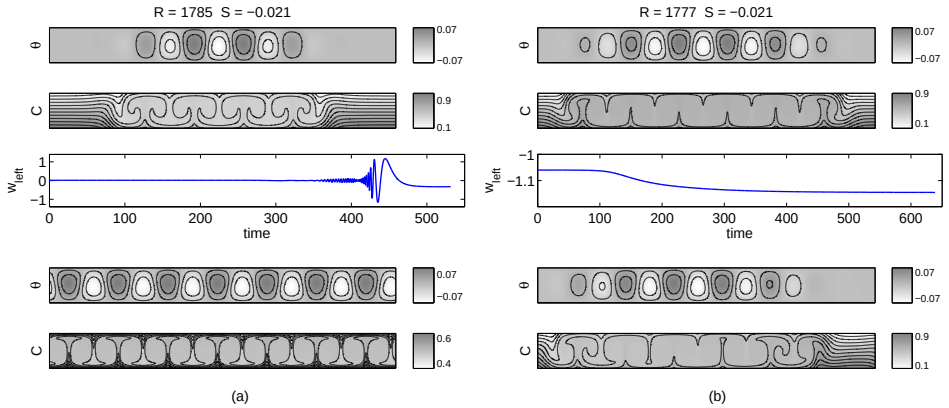

FIGURE 4. Case A. Unstable even parity convectons at (a) $e1$ ($R = 1785$) and (b) $e2$ ($R = 1777$). In each case the top panel shows the initial steady convecton, the middle panel shows the evolution of $w_{\text{left}} \equiv w(x = -4.8, z = 0.78, t)$ and the bottom panel shows the final state reached. The states are visualized in terms of contours of constant temperature fluctuation θ and contours of constant concentration C. Here and elsewhere all solution profiles use the same color table to indicate the amplitude of the temperature and concentration fields.

$R = 1777$), is numerically stable, as expected from the SH35 analysis in Fig. 3. Thus the longer convectons, that is, convectons resembling the stable periodic P_7 state over longer portions behave as expected on the basis of general theory [12] while the shorter convectons lower down on the snaking branches are typically all unstable. We surmise but have not confirmed that this loss of stability is related to the presence of the oscillatory instability of the conduction state in $R > R_H$ that is inherited by low-lying, shorter convectons.

We remark that the even convecton in Fig. 4(a), top panel, entrains lighter fluid from above, resulting in a lower than average concentration within the convecton, while the even convecton in Fig. 4(b), top panel, entrains heavier fluid from below, resulting in a higher than average concentration within. In contrast, the vortices at the two ends of the odd convecton (Fig. 4(b), bottom panel) rotate in the same sense (counterclockwise), and as a result the vortex at the right entrains heavier fluid from the bottom while that at the left entrains lighter fluid from the top, setting up a visible mean concentration gradient across the convecton.

2.2. **Case B: $\sigma = 6.86$, $\tau = 0.0083$, $S = -0.127$.** Figure 1(b) shows the corresponding results for the more negative value of the separation ratio S used in [19]. In this case the branch TW_7 bifurcates from the conduction state at $R = R_H \approx 1960.5$ and the P_7 branch only acquires stability for $R > R^* \approx 1941.5$. In this case the change of stability of the P_7 branch falls inside the pinning region [17], and this fact is expected to influence the stability properties of the higher-lying, longer convectons on L_{even} and L_{odd}. Observe that the pinning regions of the odd and even states are now noticeably different although their left boundaries coincide. This is a consequence of horizontal pumping of concentration by the odd parity states,

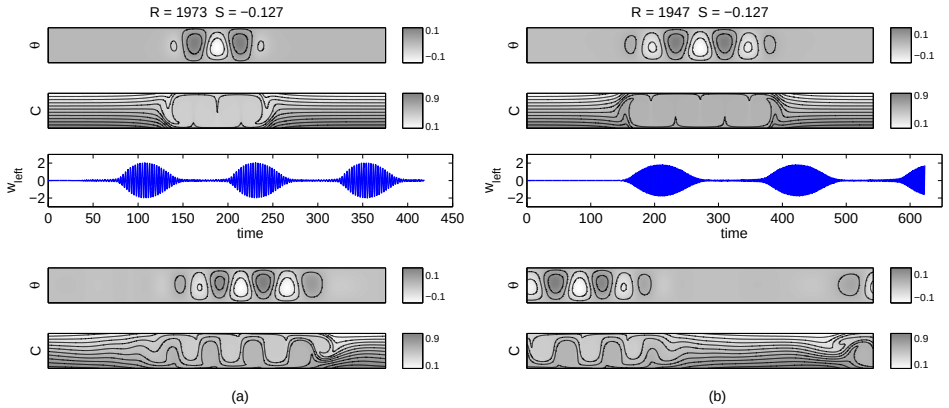

FIGURE 5. Case B. Even parity convectons at (a) $e1$ ($R = 1973$, top panel), and (b) at $e2$ ($R = 1947$, top panel), are both linearly unstable to asymmetric perturbations and evolve into spatially localized traveling waves (bottom panels).

as explained in [25, 26]. Note also that both pinning regions are broader, a fact that can be attributed to the more negative value of S. This change in S promotes subcriticality of the periodic branch P_7.

Figure 5(a) shows an even parity convecton at $e1$ in Fig. 1(b), at $R = 1973$. This portion of the branch is stable to amplitude perturbations but numerical integration shows that the state is linearly unstable to asymmetric perturbations and evolves into a localized right-traveling wave. A snapshot of this state is shown in Fig. 5(a), bottom panel. The envelope of this state drifts in the same direction as the TW within but on a much slower time scale. Figure 5(b), shows that an even convecton at $e2$ ($R = 1947$), is also unstable to asymmetric perturbations and also evolves into a localized traveling wave of the same type, this time traveling (and drifting) to the left (Fig. 6). This remains so for the convecton at $e3$ ($R = 1965.5$) (not shown) although the convecton at $e4$ ($R = 1970$) evolves into the stable P_7 state (not shown). We have not found any stable convectons for this set of parameter values.

Figure 7 shows the Nusselt number time series associated with the localized traveling waves. Both time traces are periodic, indicating that the localized traveling waves are two-frequency states – the construction of the Nusselt number removes the translation frequency of the pattern leaving only the modulation frequency [18]. The apparent period-doubling in (b) is a consequence of asymmetry between up and downflows [18].

2.3. **Case C: $\sigma = 9.16$, $\tau = 0.008$, $S = -0.257$.** Figure 8 shows the corresponding results for $S = -0.257$, a separation ratio used in [27]. In this case the pinning region is inside the instability range of P_7 ($R^* \approx 2431$) and we expect all extended localized states high up the L_{even} and L_{odd} branches to be unstable. The pinning regions are now even broader, and once again the left boundaries of the odd and even states coincide. The pumping effect responsible for the difference in the right boundaries of the odd and even pinning regions is much stronger now since a larger

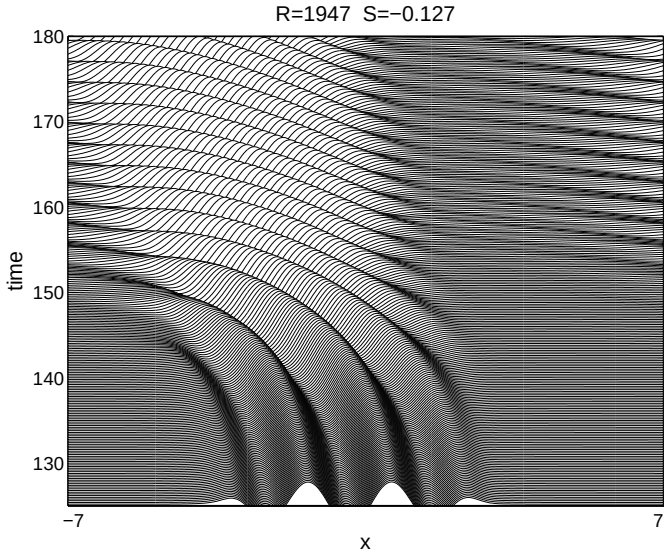

FIGURE 6. Case B. A space-time plot showing the evolution of the convecton in Fig. 5(b) into a spatially localized traveling wave. Both the waves within the packet and the packet itself travel to the left, although the speed of the latter is quite slow. Other perturbations evolve into the same state but traveling towards the right.

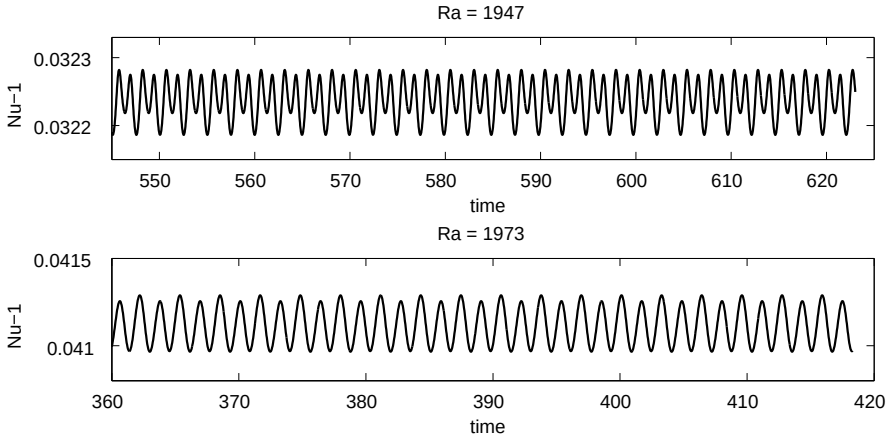

FIGURE 7. Case B. The Nusselt numbers $\mathrm{Nu} - 1 \equiv \Gamma^{-1} \int_{-\Gamma/2}^{\Gamma/2} \partial_z \theta(x, z = 1)\, dx$ as a function of time for the localized traveling waves in the bottom panels of Fig. 5. In each case the Nusselt number is periodic in time.

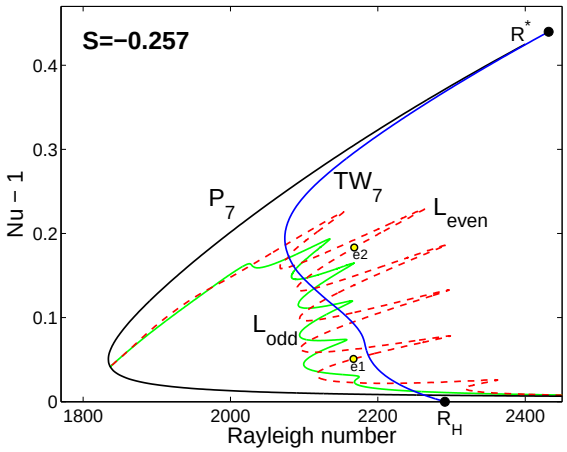

FIGURE 8. Case C. Bifurcation diagram in a periodic domain with period $\Gamma = 14$, showing the normalized convective Nusselt number $\mathrm{Nu} - 1 \equiv \Gamma^{-1} \int_{-\Gamma/2}^{\Gamma/2} \partial_z \theta(x, z = 1)\, dx$ as a function of the Rayleigh number R for stationary periodic convection (P_7) and stationary spatially localized states of even ($\mathrm{L}_{\mathrm{even}}$, dashed line) and odd ($\mathrm{L}_{\mathrm{odd}}$, solid line) parity. The branch of traveling waves (TW_7) is also shown. The P_7 branch is stable only for $R > R^*$.

value of $|S|$ implies a stronger concentration separation and hence an increase in the effectiveness of entrainment, for fixed R or equivalently fixed vortex strength.

In this case we find, as expected, that the convectons decay into a spatially periodic TW. Figure 9(a,b) shows two even convectons from $\mathrm{L}_{\mathrm{even}}$, at $e1$ ($R = 2167$) and $e2$ ($R = 2168$), of quite different lengths, selected from the pinning region, together with the results of time evolution. Although both states are amplitude-stable they are unstable to asymmetric perturbations that evolve into the TW_7 shown in the bottom panels. A careful look reveals that the TW_7 do indeed break both the even and odd symmetries of the stationary states, while retaining the mirror-glide symmetry.

3. **Summary.** In this article we have summarized the properties of strongly dissipative solitons called convectons that are found in binary fluid convection. These convectons come in two families, distinguished by their parity. We have seen that both families are organized in a snaking diagram, although in contrast to simpler systems such SH35 [12] the widths of the snaking regions of the odd and even states are different. This difference increases with increasing $|S|$ since the width of each region increases with the subcriticality of the periodic branch. We have attributed this fact to the pumping effect associated with odd parity convectons whereby heavier fluid is pumped across the convecton from one side to the other depending on the direction of the vortices in the front regions bounding the convecton.

We have seen that depending on the location of the pinning region relative to the termination R^* of the TW branch these structures can be stable, and have shown that when this is not the case the states may evolve into different types of traveling

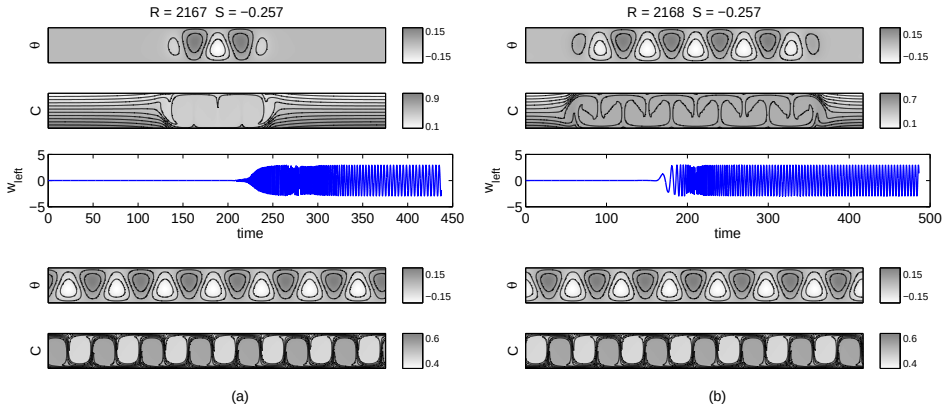

FIGURE 9. Case C. Even parity convectons on the L_{even} branch. (a) Location $e1$, $R = 2167$. (b) Location $e2$, $R = 2168$. Both convectons are amplitude-stable but unstable to asymmetric perturbations, and decay into TW_7.

states, either spatially extended or spatially localized. This richness reflects the absence of variational structure of the fluid equations. Overall the stability properties of the convectons are quite similar to those in Marangoni convection in a binary mixture with a negative separation ratio [2]. In this system short convectons are also strongly affected by their proximity to the primary Hopf bifurcation and are generally unstable, while those higher up the snaking diagram are stabilized provided the periodic state is itself stable. We hope that these results will stimulate a new series of experiments on water-ethanol mixtures. Existing experiments for $\sigma = 5.97$, $\tau = 0.0085$, $S = -0.020$ [20] have identified stable convectons embedded in a background of traveling waves but pure convectons have not been observed. For such experiments we predict that the background waves would die away as the Rayleigh number is decreased below the threshold for the absolute instability of the conduction state [5], leaving the steady convectons described here.

The states studied here are characterized by a length scale inherited from the depth of the fluid layer. In optical systems this scale is analogous to the longitudinal dimension, representing a fundamental difference between the present system and many others in which the length scale is selected by a Turing or modulational instability in the transverse direction. The behavior of the system nevertheless resembles that of simpler variational systems; this is a consequence of the fact that the snaking or pinning region is produced by transversal intersections of the stable and unstable manifolds of the conduction state and spatially periodic convection, a mechanism that is both robust and independent of the detailed structure of the equation(s) provided these are reversible in space [6, 13, 29].

REFERENCES

[1] N. Akhmediev and A. Ankiewicz (eds), "Dissipative Solitons," Lect. Notes in Physics, **661**, Springer, Berlin, 2005.

[2] P. Assemat, A. Bergeon and E. Knobloch, *Spatially localized states in Marangoni convection in binary mixtures*, Fluid Dyn. Res., **40** (2008), 852–876.

[3] W. Barten, M. Lücke, M. Kamps and R. Schmitz, *Convection in binary fluid mixtures. I. Extended traveling-wave and stationary states*, Phys. Rev. E, **51** (1995), 5636–5661.

[4] O. Batiste and E. Knobloch, *Simulations of localized states of stationary convection in ^3He-^4He mixtures*, Phys. Rev. Lett., **95** (2005), 244501.
[5] O. Batiste, E. Knobloch, A. Alonso and I. Mercader, *Spatially localized binary-fluid convection*, J. Fluid Mech., **560** (2006), 149–158.
[6] M. Beck, J. Knobloch, D. J. B. Lloyd, B. Sandstede and T. Wagenknecht, *Snakes, ladders, and isolas of localized patterns*, SIAM J. Math. Anal., **41** (2009), 936–972.
[7] A. Bergeon and E. Knobloch, *Spatially localized states in natural doubly diffusive convection*, Phys. Fluids, **20** (2008), 034102.
[8] A. Bergeon, J. Burke, E. Knobloch and I. Mercader, *Eckhaus instability and homoclinic snaking*, Phys. Rev. E, **78** (2008), 046201.
[9] S. Blanchflower, *Magnetohydrodynamic convectons*, Phys. Lett. A, **261** (1999), 74–81.
[10] S. Blanchflower and N. O. Weiss, *Three-dimensional magnetohydrodynamic convectons*, Phys. Lett. A, **294** (2002), 297–303.
[11] C. S. Bretherton and E. A. Spiegel, *Intermittency through modulational instability*, Phys. Lett. A, **96** (1983), 152–156.
[12] J. Burke and E. Knobloch, *Snakes and ladders: Localized states in the Swift-Hohenberg equation*, Phys. Lett. A, **360** (2007), 681–688.
[13] P. Coullet, C. Riera and C. Tresser, *Stable static localized structures in one dimension*, Phys. Rev. Lett., **84** (2000), 3069–3072.
[14] J. H. P. Dawes, *Localized convection cells in the presence of a vertical magnetic field*, J. Fluid Mech., **570** (2007), 385–406.
[15] Q. Feng, J. V. Moloney and A. C. Newell, *Transverse patterns in lasers*, Phys. Rev. A, **50** (1994), 3601–3604.
[16] K. Ghorayeb and A. Mojtabi, *Double diffusive convection in a vertical rectangular cavity*, Phys. Fluids, **9** (1997), 2339–2348.
[17] D. Jung and M. Lücke, *Bistability of moving and self-pinned fronts of supercritical localized convection structures*, Europhys. Lett., **80** (2007), 14002, 1–6.
[18] E. Knobloch, A. E. Deane, J. Toomre and D. R. Moore, *Doubly diffusive waves*, in "Multiparameter Bifurcation Theory" (eds. M. Golubitsky and J. Guckenheimer), Contemp. Math., **56** (1986), American Mathematical Society, Providence, R.I., 203–216.
[19] P. Kolodner, *Observations of the Eckhaus instability in one-dimensional traveling-wave convection*, Phys. Rev. A, **46** (1992), 1739–1742.
[20] P. Kolodner, *Coexisting traveling waves and steady rolls in binary-fluid convection*, Phys. Rev. E, **48** (1993), R665–668.
[21] P. Kolodner, J. A. Glazier and H. L. Williams, *Dispersive chaos in one-dimensional traveling-wave convection*, Phys. Rev. Lett., **65** (1990), 1579–1582.
[22] I. Mercader, A. Alonso and O. Batiste, *Numerical analysis of the Eckhaus instability in travelling-wave convection in binary mixtures*, Eur. Phys. J. E, **15** (2004), 311–318.
[23] I. Mercader, A. Alonso and O. Batiste, *Spatiotemporal dynamics near the onset of convection for binary mixtures in cylindrical containers*, Phys. Rev. E, **77** (2008), 036313.
[24] I. Mercader, O. Batiste and A. Alonso, *Continuation of travelling-wave solutions of the Navier-Stokes equations*, Int. J. Num. Methods in Fluids, **52** (2006), 707–721.
[25] I. Mercader, O. Batiste, A. Alonso and E. Knobloch, *Localized pinning states in closed containers: Homoclinic snaking without bistability*, Phys. Rev. E, **80** (2009), 025201(R).
[26] I. Mercader, O. Batiste, A. Alonso and E. Knobloch, *Convectons in periodic and bounded domains*, Fluid Dyn. Res., **42** (2010), 025505.
[27] D. R. Ohlsen, S. Y. Yamamoto, C. M. Surko and P. Kolodner, *Transition from traveling-wave to stationary convection in fluid mixtures*, Phys. Rev. Lett., **65** (1990), 1431–1434.
[28] Y. Pomeau, *Front motion, metastability and subcritical bifurcations in hydrodynamics*, Physica D, **23** (1986), 3–11.
[29] P. D. Woods and A. R. Champneys, *Heteroclinic tangles and homoclinic snaking in the unfolding of a degenerate reversible Hamiltonian Hopf bifurcation*, Physica D, **129** (1999), 147–170.

Received July 2009; revised January 2010.

E-mail address: isabel@fa.upc.edu
E-mail address: oriol@fa.upc.edu
E-mail address: arantxa@fa.upc.edu
E-mail address: knobloch@berkeley.edu